Effect of resonant helical magnetic fields on plasma rotation

Q. Yu[1], S. Günter[1] and K. H. Finken[2]

[1]Max-Planck-Institut für Plasmaphysik, EURATOM Association, 85748 Garching, Germany

[2]Institute of Energy Research - Plasma Physics, Forschungszentrum Jülich GmbH, Association EURATOM-FZJ, Trilateral Euregio Cluster, 52425 Jülich, Germany

The effect of a resonant helical magnetic field on plasma rotation is investigated numerically based on the two fluid equations. It is found that, depending on the frequency and the direction of the original plasma rotation, a static helical field of a small amplitude can either increase or decrease the rotation speed. With increasing the field amplitude, the plasma rotation frequency approaches the electron diamagnetic drift frequency but rotates in the ion drift direction. These results provide a new understanding of the recent experimental observations of TEXTOR [K.H. Finken *et al.*, Phys. Rev. Letts, **94**, 015003(2005)].

PACS: 52.35.Py, 52.35.Vd, 52.55.Tn, 52.35.-g

I. Introduction

The effect of resonant helical magnetic fields on plasma confinement is of great interest to plasma physics research. Three subtopics are of particular concern for a fusion reactor:

(a) Helical field penetration: For the plasma being originally stable to tearing modes, an applied resonant helical field (or error fields of experimental devices) can penetrate through the resonant surface and generate a magnetic island there [1-9]. Recently it was shown on TEXTOR that the relative frequency between the mode and the helical field is important in determining the field penetration [5,6], being in agreement with theoretical results [7-9].

(b) Mode locking: The locking of large magnetic islands by error fields is often observed in experiments, leading to severe confinement degradation in tokamak plasmas or even to disruptions [1,10,11]. The mode locking threshold is predicted to be much lower in a fusion reactor than in existing tokamaks due to the stronger magnetic field and lower plasma rotation speed [12].

(c) Edge localized modes (ELMs) mitigation: Helical fields were found to be able to control ELMs while maintaining the pedestal and the confinement of H-mode plasmas, being planned to be applied in ITER [13].

One puzzle arising from the experimental results is the effect of a helical field on plasma rotation. Increased bulk plasma rotation due to an applied static helical field before field penetration was observed on TEXTOR [6]. The tentative explanation for this phenomenon was the induced radial electric field in a stochastic magnetic field generated by the helical field, which leads to the same rotation direction as seen in the experiments [6]. This explanation, however, faces the problem that there is little field ergodicity before field penetration. A change of the bulk plasma rotation from the electron diamagnetic drift direction to the ion's direction by a static penetrated helical field was also observed in experiments [1], a phenomenon not well understood yet. In the framework of reduced MHD equations the static field is known to slow down the bulk plasma rotation [1,7,10].

Recently, two fluids equations were utilized to study helical field penetration [8,9,14], including the linear study on the effect of a rotating helical field on plasma rotation [9]. As plasma rotation is very important for, e.g., the stability of the resistive wall modes, a better understanding of the experimental results given in Ref. 1 and 6 is desirable. In this paper the effect of a static helical field on plasma rotation is investigated numerically using the (reduced) nonlinear two fluid equations. The obtained results show the same features as observed in the experiments [1,6].

II. Computational model

The large aspect-ratio tokamak approximation is utilized. The magnetic field is defined as $\mathbf{B}=B_{0t}\mathbf{e}_t-(k_t/k_\theta)B_{0t}\mathbf{e}_\theta+\nabla\psi\times\mathbf{e}_t$, where ψ is the helical flux function, $k_\theta=m/r$ and $k_t=n/R$ are the wave vector in $\mathbf{e}_\theta$ (poloidal) and $\mathbf{e}_t$ (toroidal) direction, r and R are the minor and the major radius, m and n are the poloidal and toroidal mode numbers of the helical field, and the subscript 0 denotes an equilibrium quantity. The plasma velocity is given by $\mathbf{v}=v_\parallel\mathbf{e}_\parallel+\nabla\phi\times\mathbf{e}_t$, where ϕ is the stream function.

The two fluid equations utilized here include the generalized Ohm's law, the equation of motion in the perpendicular (after taking $\nabla\times$) and the parallel (to magnetic field) direction, and the energy and the mass conservation equations. Normalizing the length to the minor radius a, the time t to the resistive time $\tau_R=a^2\mu_0/\eta$, the helical flux ψ to aB_{0t}, $\mathbf{v}$ to a/τ_R, and the electron temperature T_e and density n_e to their values at the magnetic axis, theses equations become

$$\frac{d\psi}{dt}=E-\eta j+\Omega(\nabla_\parallel n_e+\nabla_\parallel T_e) \tag{1}$$

$$\frac{dU}{dt}=-S^2\nabla_\parallel j+\mu\nabla_\perp^2 U+S_m \tag{2}$$

$$\frac{dv_\parallel}{dt}=-c_s^2\nabla_\parallel P/n_e+\mu\nabla_\perp^2 v_\parallel \tag{3}$$

$$\frac{3}{2}n_e\frac{dT_e}{dt} = 0.78(\Omega/\beta)\nabla_{\parallel}j + T_e n_e \nabla_{\parallel} v_{\parallel} + n_e \nabla_{\parallel}(\chi_{\parallel}\nabla_{\parallel}T_e) + n_e \nabla_{\perp}(\chi_{\perp}\nabla_{\perp}T_e) + S_p \quad (4)$$

$$\frac{dn_e}{dt} = (\Omega/\beta)\nabla_{\parallel}j - \nabla_{\parallel}(n_e v_{\parallel}) + \nabla_{\perp}(D_{\perp}\nabla_{\perp}n_e) + S_n \quad (5)$$

where $d/dt=\partial/\partial t+\mathbf{v}_{\perp}\cdot\nabla_{\perp}$, $j=\nabla_{\perp}^2\psi-2k_tB_{0t}/mR$ being the toroidal plasma current density, η is the normalized resistivity, E is the equilibrium electric field, $\Omega=\beta d_1$, $\beta=4\pi p_e/B^2$, $p_e=n_eT_e$, $d_1=\omega_{ce}/\nu_e$, and ω_{ce} and ν_e are the electron cyclotron and the collisional frequency. $S=\tau_R/\tau_A$, where $\tau_A=a/V_A$ being the toroidal Alfven time. $U=-\nabla_{\perp}^2\phi$ is the plasma vorticity, $c_s=(T_e/m_i)^{1/2}$, μ the plasma viscosity, and $\chi_{\parallel}$, $\chi_{\perp}$ and $D_{\perp}$ are the parallel and perpendicular heat and particle diffusivity. S_p is the heating power, S_n is the particle source, and S_m is the poloidal momentum source given by

$$S_m = \Omega_E[1-(r/a)^2]^3, \quad (6)$$

which leads to an equilibrium poloidal plasma rotation. Cold ion assumption is made here since the ion temperature is significantly lower than the electron's in the considered experiments [5,6].

III. Numerical Results

Equations (1)-(5) are solved simultaneously using the initial value code TM1, which has been used for modelling drift tearing modes and neoclassical tearing modes [15-16]. Dedicated numerical methods are utilized in the code to reduce the numerical error [17,18].

The calculations are performed for a single helicity perturbation with m/n=2/1. The effect of the helical field is taken into account by the boundary condition

$$\psi_{m/n}(r=a) = \psi_a\cos(m\theta+n\phi), \quad (7)$$

where ψ_a describes the helical magnetic flux amplitude of the m/n component at r=a.

The input parameters are based on TEXTOR experimental parameters. The toroidal magnetic field is B_{0t}=2.5T, and the plasma minor and major radius are a=0.47m and R=1.75m, respectively. The equilibrium electron temperature and density profiles are modeled by T_e=1.8[1-

$(r/a)^2]^{1.2}$+0.3 (keV), and n_e=3.2[1-$(r/a)^2]^{1.5}$+0.3 ($10^{19}m^{-3}$) [5,6,9]. These parameters lead to $S=1.97\times10^8$, $\Omega=6.3\times10^4$, $c_s=1.2\times10^7$ (a/τ_R), $d_1=2.5\times10^7$, and $\chi_{\parallel}=1.1\times10^9$ (a^2/τ_R). Here $\chi_{\parallel}=v_{Te}/k_{\parallel}$ is used for calculating $\chi_{\parallel}$, and v_{Te} is the electron thermal velocity [19]. The precise form of $\chi_{\parallel}$ for a high temperature plasma is more complex as discussed in Ref. [19].

Assuming the perpendicular heat diffusivity and the plasma viscosity to be at the anomalous transport level $0.5m^2/s$, one finds $\chi_{\perp}=\mu=21(a^2/\tau_R)$ in normalized units. Furthermore, $D_{\perp}=\chi_{\perp}/5$ is taken. These parameters are used as input for our calculations except mentioned elsewhere. A monotonic profile of the safety factor q is used, and the q=2 rational surface locates at r_s=0.628a in agreement with the experiments [5,6,9]. The m/n=2/1 tearing mode is stable without an externally applied helical field.

For simplicity, we first study the case with a constant electron temperature. With different initial equilibrium plasma rotation velocities, the effect of a helical field on the plasma rotation is different. The radial profiles of the (normalized) m/n=0/0 component of the poloidal plasma rotation velocity, V_θ, in steady state are shown in figure 1 for two cases: (a) $\omega_0\equiv-\omega_{E0}/\omega_{*e0}$=0.42 (black curves) with $\psi_a=10^{-5}$ (solid) and 0 (dashed). (b) ω_0=-0.42 (red) with $\psi_a=0.4\times10^{-5}$ (solid) and 1.14×10^{-5} (dotted) and 0 (dashed), where ω_{E0} and ω_{*e0} are the original equilibrium plasma rotation frequency and the electron diamagnetic drift frequency at the rational surface. The ω_0 values are also marked near the corresponding curves in the figure. The positive (negative) value of ω_0 refers to the rotation in the the ion (electron) diamagnetic drift direction. It is seen that the rotation is speeded up by the static helical field for ω_0=0.42, while for ω_0=-0.42 the rotation first slows down (for $\psi_a=0.4\times10^{-5}$) and then changes its direction to the ion diamagnetic drift direction for larger helical field amplitude ($\psi_a=1.14\times10^{-5}$). These results are consistent with the experimental observations [1,6]. For ω_0>1 the plasma rotation velocity is always found to decrease.

The results shown in Fig. 1 can be understood from the generalized Ohm's law. Assuming the perturbed helical flux $\psi_1 \sim \exp[i(-\omega t+m\theta+n\phi)]$, for a sufficiently small ψ_a it is found from Eq. (1) that in the lowest order the toroidal current perturbation at the rational surface r_s is given by

$$j_1(r_s) = i(\omega-\omega_E-\omega_{*e})\psi_1/\eta \tag{8}$$

where the subscript 1 denotes perturbed quantities, ω is the mode frequency, $\omega_E=V_\theta m/r$ being the frequency due to V_θ, $\omega_{*e}=V_{*et}n/R=V_{*e\theta}m/r$ being the frequency due to the electron diamagnetic drift, $V_{*et}=p_e'/n_eeB_{0\theta}$, $V_{*e\theta}=-p_e'/n_eeB_{0t}$, and the prime denotes d/dr.

The current perturbation together with the radial magnetic field perturbation, b_{r1}, leads to a poloidal electromagnetic torque of the m/n=0/0 component, $T_{0/0}=r(j_1^*b_{r1}+j_1b_{r1}^*)/2$, where the superscript * refers to the complex conjugated part. At the rational surface one finds

$$T_{0/0}(r_s) = m(\omega-\omega_E-\omega_{*e})|\psi_1|^2/\eta. \tag{9}$$

As the mode frequency is given by the applied field frequency, for a static helical field $\omega=0$. Eq. (9) is then reduced to

$$T_{0/0}(r_s) = -m\omega_E(1+\omega_{*e}/\omega_E)(|\psi_1|)^2/\eta. \tag{10}$$

In the MHD limit $\omega_{*e}=0$ is used, and $T_{0/0}(r_s)$ is further simplified to $-m\omega_E(|\psi_1|)^2/\eta$, which is always opposite to the plasma rotation direction, slowing down the rotation speed, no matter in which direction the plasma originally rotates.

When taking into account the electron diamagnetic drift, the torque direction depends on the rotation frequency and direction. Eq. (10) indicates that for $(1+\omega_{*e}/\omega_E)<0$ (plasma rotates in the ion drift direction with a frequency smaller than ω_{*e}), the torque is in the rotation direction. For $(1+\omega_{*e}/\omega_E)>0$, however, the torque is in the opposite direction.

The above analysis is consistent with numerical results. Corresponding to Fig. 1, the radial profiles of $T_{0/0}$ in steady state are shown in figure 2 for $\omega_0=0.42$ (black curve) and 2.08 (blue) with $\psi_a=0.4\times10^{-5}$. The red curves are for $\omega_0=-0.42$ with $\psi_a=0.4\times10^{-5}$ (solid) and 1.14×10^{-5} (dotted).

The ω_0 values are also marked near the corresponding curves in the figure. The torque peaks at the rational surface and is in the plasma rotation direction for ω_0=0.42 (see Fig. 1) but is opposite to the rotation direction for ω_0=2.08, as expected. For ω_0=-0.42 the torque is also directed opposite to the plasma rotation for a small ψ_a, and it even changes the rotation direction for $\psi_a=1.14\times10^{-5}$. The torque direction is as predicted by Eq. (10) for all cases.

For a small helical field amplitude, the electromagnetic torque is localized around the rational surface and tends to modify the local plasma rotation velocity. The plasma viscosity, however, will response to the local velocity change and tend to keep the neighbouring plasma to rotate together with the local plasma at the rational surface. This results in a more global change in the rotation velocity profile, as seen from Fig. 1, such that the electromagnetic torque is balanced by the viscous torque. With increasing helical field amplitude, the electromagnetic torque becomes larger as seen from Eq. (10), and it will eventually lead to $\omega_E\approx-\omega_{*e}$ at the rational surface for a static helical field, such that electromagnetic torque is not too large to be balanced by the viscous torque. In this case the global rotation velocity profile also significantly changes.

For a systematic study, the normalized plasma rotation frequency, $\omega_{En}\equiv-\omega_E/\omega_{*e0}$ (solid curve), and the normalized electron diamagnetic drift frequency, $\omega_{*en}\equiv\omega_{*e}/\omega_{*e0}$ (dotted curve), at the rational surface in steady state are shown as a function of ψ_a in figure 3 for three cases, ω_0=0.42 (black curve), 2.08 (blue) and -0.42 (red). The ω_0 value for these curves can be also found from the ω_{En} value at ψ_a =0. The dashed curve shows the normalized island width w/a multiplied by a factor 10. It is seen that for ω_0=0.42, the normalized rotation frequency ω_{En} first increases with increasing ψ_a and then decreases following the decrease of ω_{*en}. For a sufficiently large ψ_a or island width, the plasma density gradient decreases in the island region due to the parallel transport, and therefore ω_{*e} decreases. The sudden increase in the island width corresponds to the helical field penetration. For ω_0=2.08 the normalized frequency ω_{En} decreases

towards ω_{*en}. With ω_0=-0.42, ω_{En} increases from a negative value to approach ω_{*en}. No matter what is the initial rotation speed or direction, the nonlinear state $\omega_{En}\approx\omega_{*en}$ (or $\omega_E\approx-\omega_{*e}$, plasma rotates in the ion drift direction) is always reached for a sufficiently large ψ_a. In this state the torque is minimum as seen from Eq. (10).

For a non-constant electron temperature, similar results are found as shown in figure 4, in which ω_{En} (solid curve) and ω_{*en} (dotted) are shown as a function of ψ_a for ω_0=0. The black (red) curves are for constant (non-constant) electron temperature. The dashed curve shows 10×w/a. The case with a non-constant electron temperature has a larger values of ω_{En} and ω_{*en} but a smaller value of w/a. A larger ψ_a is required for the field penetration with a non-constant electron temperature, since the frequency difference between the mode and the field is larger due to the contribution of the temperature gradient to ω_{*e}. It is seen that a static field forces the plasma to rotate in the ion diamagnetic drift direction, even if originally there is no plasma rotation.

In figure 5 the normalized frequencies ω_{En} (solid curve) and ω_{*en} (dotted curve) are shown as a function of log(S) for ω_0=0 and $\psi_a=10^{-5}$. The other parameters are the same as those of Fig. 3. The dashed curve shows 10×w/a. The electromagnetic torque exerted on the island by the helical field is larger for a larger magnetic Renolds number S, so that ω_{En} increases with increasing S, which in turn leads to field penetration at $S=1.2\times10^8$ as indicated by a sudden increase in the island width. After field penetration one finds $\omega_E\approx-\omega_{*e}$ similar to the results shown in Figs. 3 and 4, and $\omega_{*e}\approx0.9\omega_{*e0}$ due to the small island width. Fig. 5 suggests that the plasma rotation will be more easily generated by the helical field for a reactor plasma with a high S value.

IV. Discussion and Summary

The above results are obtained for the case of poloidal plasma rotation. In tokamak experiments the plasma rotation is mostly in the toroidal direction due to the neoclassical effect

not considered here. For toroidal rotation, Eq. (9) is found to be modified as

$$T_{0/0}(r_s)=n(\omega-\omega_E-\omega_{*e})|\psi_1|^2/\eta, \qquad (11)$$

where $\omega_E=V_t n/R$ being the mode frequency due to the toroidal plasma rotation velocity V_t. The electron diamagnetic drift is in the counter plasma current direction, so that the helical field drives the plasma to rotates in the co-current direction. A larger toroidal rotation speed than the poloidal one will be driven by the helical field, since the toroidal rotation speed should be $(m/n)(R/r_s)$ times larger than the poloidal one for the same change in the frequency.

Our results indicates that a static resonant magnetic perturbation of a single helicity can drive plasma flow, showing the same features as observed in the experiments [1,6]. Future studies using the toroidal rotation and a stochastic magnetic field will be helpful for a further comparison with the experimental results.

For a fusion reactor the plasma rotation velocity is expected to be low, since the neutral beam injection heating will not be present for a burning plasma. A slowly rotating plasma will be more easily subject to plasma instabilities due to the weaker stabilizing effect of the wall. As the diamagnetic drift velocity is very large in the pedestal region of H-mode plasmas, while the local parallel transport is not too fast, a local fast plasma rotation could be generated by a static helical field of an appropriate amplitude, especially when considering the reduced plasma viscosity in the pedestal region. Spontaneous plasma rotation in the co-current direction has been found in H-mode plasmas on several tokamaks [20]. It would be of interest to study whether the intrinsic machine error field is resonant at the plasma edge and large enough to cause such a rotation. In the tokamak core region the parallel transport is much faster, and ω_{*e} begins to decrease due to the flattening of the radial electron pressure profile even before field penetration [8]. In this case a rotating helical field would still be able to drive plasma rotation. Eqs. (9) and (11) suggest that a helical field rotating in the ion diamagnetic drift direction can more efficiently drive plasma rotation. This was indeed found to be the case in TEXTOR experimental results [6].

In summary, the effect of a resonant helical field on plasma rotation is investigated based on two fluid equations, providing a new insight into previous experimental results. It is found that: (a) Before field penetration the rotation is speeded up by a static helical field in case the original rotation is in the ion diamagnetic drift direction with a frequency smaller than ω_{*e}, but it is slowed down otherwise. (b) For a sufficiently large field amplitude, the plasma rotation frequency approaches the electron diamagnetic drift frequency but rotates in the ion drift direction.

References

[1] T.C. Hender, R. Fitzpatrick, A.W. Morris, P.G. Carolan, R.D. Durst, T. Edlington, J. Ferreira, S.J. Fielding, P.S. Haynes, J. Hugill, I.J. Jenkins, R.J. La Haye, B.J. Parham, D.C. Robinson, T.N. Todd, M. Valovic and G. Vayakis, Nucl. Fusion **32**, 2091 (1992).

[2] R.J. Buttery, M. De' Benedetti, T.C. Hender and B.J.D. Tubbing, Nucl. Fusion **40**, 807 (2000).

[3] R. J. La Haye, R. Fitzpatrick, T. C. Hender, A. W. Morris, J. T. Scoville, and T. N. Todd, Phys. Fluids B **4**, 2098 (1992).

[4] S. M. Wolfe, I. H. Hutchinson, R. S. Granetz, J. Rice, and A. Hubbard, Phys. Plasmas **12**, 056110 (2005).

[5] H.R. Koslowski, Y. Liang, A. Krämer-Flecken, K. Löwenbrück, M. von Hellermann, E. Westerhof, R. C. Wolf, O. Zimmermann and the TEXTOR team, Nucl. Fusion **46**, L1 (2006).

[6] K. H. Finken, S. S. Abdullaev, M. F. M. de Bock, M. von Hellermann, M. Jakubowski, R. Jaspers, H. R. Koslowski, A. Krämer-Flecken, M. Lehnen, Y. Liang, A. Nicolai, R. C. Wolf, O. Zimmermann, M. de Baar, G. Bertschinger, W. Biel, S. Brezinsek, C. Busch, A. J. H. Donné, H. G. Esser, E. Farshi, H. Gerhauser, B. Giesen, D. Harting, J. A. Hoekzema, G. M. D. Hogeweij, P. W. Hüttemann, S. Jachmich, K. Jakubowska, D. Kalupin, F. Kelly, Y. Kikuchi, A. Kirschner, R. Koch, M. Korten, A. Kreter, J. Krom, U. Kruezi, A. Lazaros, A. Litnovsky, X. Loozen, N. J. Lopes Cardozo, A. Lyssoivan, O. Marchuk, G. Matsunaga, Ph. Mertens, A. Messiaen, O. Neubauer, N. Noda, V. Philipps, A. Pospieszczyk, D. Reiser, D. Reiter, A. L. Rogister, M. Sakamoto, A. Savtchkov, U. Samm, O. Schmitz, R. P. Schorn, B. Schweer, F. C. Schüller, G. Sergienko, K. H. Spatschek, G. Telesca, M. Tokar, R. Uhlemann, B. Unterberg, G. Van Oost, T. Van Rompuy, G. Van Wassenhove, E. Westerhof, R. Weynants, S. Wiesen, and Y. H. Xu, Phys. Rev. Letts, **94**, 015003(2005).

[7] R. Fitzpatrick, Nucl. Fusion **33**, 1049 (1993).

[8] Q. Yu, S. Günter, Y. Kikuchi, and K. H. Finken, Nuclear Fusion **48**, 024007 (2008).

[9] Kikuchi, M. F. M. de Bock, K. H. Finken, M. Jakubowski, R. Jaspers, H. R. Koslowski, A. Kraemer-Flecken, M. Lehnen, Y. Liang, G. Matsunaga, D. Reiser, R. C. Wolf, and O. Zimmermann, Phys. Rev. Letts, **97**, 085003(2006).

[10] M.F.F. Nave and J.A. Wesson, Nucl. Fusion **30**, 2575 (1990).

[11] H. Zohm, A. Kallenbach, H. Bruhns, G. Fussmann, Europhys. Lett. **11**, 745 (1990).

[12] Q. Yu and S. Günter, Nucl. Fusion **48**, 065004 (2008).

[13] T. E. Evans, R. A. Moyer, P. R. Thomas, J. G. Watkins, T. H. Osborne, J. A. Boedo, E. J. Doyle, M. E. Fenstermacher, K. H. Finken, R. J. Groebner, M. Groth, J. H. Harris, R. J. La Haye, C. J. Lasnier, S. Masuzaki, N. Ohyabu, D. G. Pretty, T. L. Rhodes, H. Reimerdes, D. L. Rudakov, M. J. Schaffer, G. Wang, and L. Zeng, Phys. Rev. Letts, **92**, 235003 (2004).

[14] F. L. Waelbroeck, Phys. Plasmas **10**, 4040 (2003).

[15] Q. Yu, S. Günter and Bruce D. Scott, Phys. Plasmas **10**, 797(2003).

[16] Q. Yu, S. Günter and K. Lackner, Phys. Plasmas **11**, 140(2004).

[17] S. Günter, Q. Yu, J. Krüger, and K. Lackner, J. Comp. Phys. **209**, 35 (2005)

[18] Q. Yu, Phys. Plasmas **13** 062310 (2006)

[19] Z. Chang and J.D. Callen, Phys. Fluids **B4**, 1167(1992).

[20] J.E. Rice, A. Ince-Cushman, J.S. deGrassie, L.-G. Eriksson, Y. Sakamoto, A. Scarabosio, A. Bortolon, K.H. Burrell, B.P. Duval, C. Fenzi-Bonizec, M.J. Greenwald, R.J. Groebner, G.T. Hoang, Y. Koide, E.S. Marmar, A. Pochelon and Y. Podpaly, Nucl. Fusion 47, 1618 (2007).

CAPTION

Figure 1 (color online) Radial profiles of the normalized m/n=0/0 component poloidal velocity, V_θ, for two cases: (a) $\omega_0 \equiv -\omega_{E0}/\omega_{*e0}=0.42$ (black curves) with $\psi_a=10^{-5}$ (solid) and 0 (dashed). (b) $\omega_0=-0.42$ (red) with $\psi_a=0.4\times10^{-5}$ (solid) and 1.14×10^{-5} (dotted) and 0 (dashed). The ω_0 values are also marked near the corresponding curves.

Figure 2 (color online) Radial profiles of $T_{0/0}$ in steady state for $\omega_0=0.42$ (black curve) and 2.08 (blue) with $\psi_a=0.4\times10^{-5}$. The red curves are for $\omega_0=-0.42$ with $\psi_a=0.4\times10^{-5}$ (solid) and 1.14×10^{-5} (dotted). The ω_0 values are also marked near the corresponding curves.

Figure 3 (color online) $\omega_{En}\equiv-\omega_E/\omega_{*e0}$ (solid curve), $\omega_{*en}\equiv\omega_{*e}/\omega_{*e0}$ (dotted) and 10w/a (dashed) versus ψ_a for $\omega_0=0.42$ (black), 2.08 (blue) and -0.42 (red). $\omega_{En}\approx\omega_{*en}$ (or $\omega_E\approx-\omega_{*e}$) for a sufficiently large ψ_a. The ω_0 value for these curves can be also found from the ω_{En} value at $\psi_a=0$.

Figure 4 (color online) ω_{En} (solid curve), ω_{*en} (dotted) and 10w/a (dashed) versus ψ_a for $\omega_0=0$. The black (red) curves are for a constant (non-constant) electron temperature. The case with a non-constant electron temperature has a larger values of ω_{En} and ω_{*en} but a smaller value of w/a. A static field drives the plasma rotation in the ion diamagnetic drift direction.

Figure 5 (color online) ω_{En} (solid curve), ω_{*en} (dotted) and 10w/a (dashed) versus log(S) for $\psi_a=10^{-5}$ and $\omega_0=0$. ω_{En} increases with increasing S. After field penetration $\omega_E\approx-\omega_{*e}$.

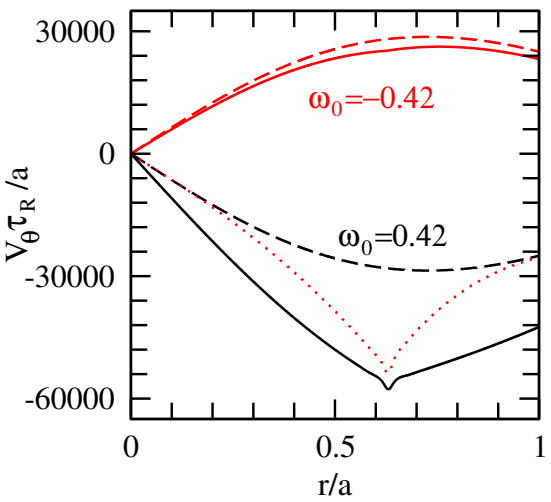
30000
0
-30000
-60000
0
0.5
1
r/a
$V_\theta \tau_R$ /a
ω_0=–0.42
ω_0=0.42

Figure 1

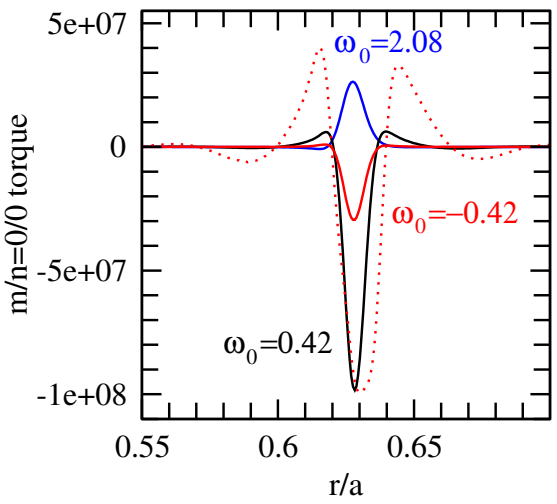

Figure 2

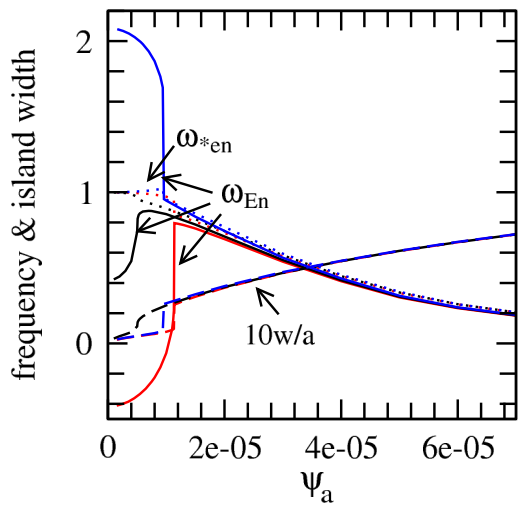

Figure 3

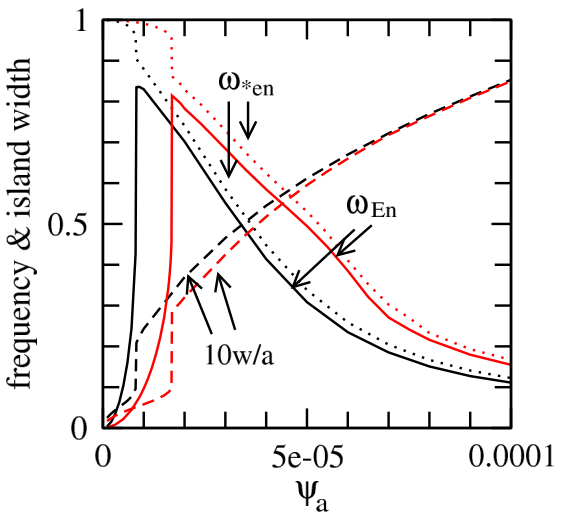

Figure 4

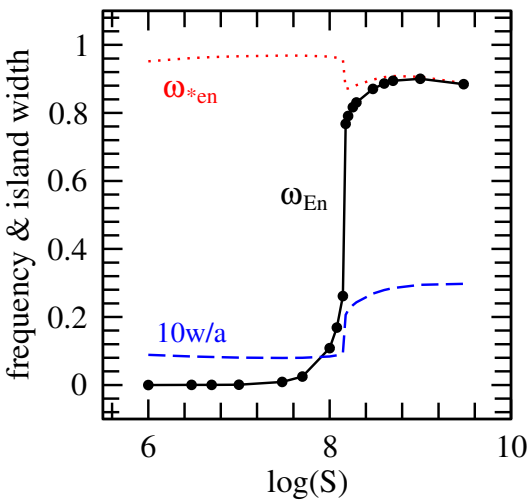

Figure 5